International Journal of Adhesion & Adhesives 39 (2012) 33–41

Contents lists available at SciVerse ScienceDirect

International Journal of Adhesion & Adhesives

journal homepage: www.elsevier.com/locate/ijadhadh

Study on the role of laser surface irradiation on damage and decohesion of Al/epoxy joints

Marco Alfano [a,*,1], Gilles Lubineau [a], Franco Furgiuele [b], Glaucio H. Paulino [c]

[a] COHMAS Laboratory, Division of Physical Science and Engineering, King Abdullah University of Science and Technology (KAUST), Thuwal 23955-6900, Kingdom of Saudi Arabia
[b] Department of Mechanical Engineering, University of Calabria, Via P. Bucci 44C, 87036 Rende (CS), Italy
[c] Department of Civil and Environmental Engineering, University of Illinois at Urbana-Champaign, 205 N. Matthew Avenue, Urbana, IL 61801, USA

ARTICLE INFO

Article history:
Accepted 1 March 2012
Available online 23 June 2012

Keywords:
Epoxy
Surface treatment
Contact angle
Fracture

ABSTRACT

In this work we investigate the effect of laser irradiation on the bond toughness of aluminum/epoxy bonded joints. The evolution of substrate surface morphology and wettability, for various sets of laser process parameters (i.e. laser power, line spacing, scan speed), was investigated by means of Scanning Electron Microscopy (SEM) and contact angle measurements. A proper combination of power, line spacing and scan speed was then selected and adhesive bonded Al/epoxy T-peel joints were prepared and tested. For comparison, similar samples were produced using substrates with classical grit blasting surface treatment. Finally, post-failure SEM analyses of fracture surfaces were performed, and in order to typify the increase in bond toughness of the joints, finite element simulations were carried out using a potential based cohesive zone model of fracture.

1. Introduction

Adhesive bonding is nowadays an established technology widely employed to join similar or dissimilar materials in a variety of modern industries (e.g. automotive, aerospace, etc.) [1–3]. The strength of adhesive joints is influenced by many factors (e.g. adherent type, bond-line thickness), but surface contamination and imperfect preparation are the foremost reasons for their compromise. The surface layer of lightweight alloys is indeed affected by the presence of contaminants, such as corrosion inhibitors, lubricants, or brittle oxides. Therefore the creation of reliable adhesive bonds requires adequate surface preparation.

A candidate surface treatment for adhesive bonded metal joints should allow the liquid adhesive to easily spread over substrate surface (i.e. improved wettability) promoting intimate molecular interaction and physical adsorption. Moreover, the resulting morphology of the treated substrates should favor mechanical interlocking. Various techniques are currently used to improve wetting of solid materials; they typically involve modification of surface chemistry and topography by means of mechanical or chemical pre-treatments [1,2,4]. Mechanical pre-treatments, such as abrasion and grit-blasting, are the oldest and most common surface preparation techniques; they enhance joints strength by increasing the surface area available for bonding and promoting mechanical interlocking at the adhesive/substrate interface. However, operators may introduce dissimilarities across the treated surfaces, and therefore substantial scatter is often observed in the experimental determination of joint strength [1,2,5]. For this reason there is low confidence in the application of mechanical pre-treatments for technically demanding applications. As an alternative, chemical pre-treatments, such as chromic–sulfuric acid etching, chromic or phosphoric acid anodizing, etc., may be applied. Most of them are wet treatments, requiring the metals to be exposed to liquid organic solvents and/or inorganic solutions [4]. They do affect substrate morphology by the formation of (1) a rough fibrillated surface which improves mechanical interlocking and/or (2) a porous oxide layer which favors chemical interaction with the adhesive [1]. However, chemical pre-treatments pose health, safety and ecological concerns. For instance, in a recent directive concerning the End-Of-Life Vehicles regulation (2000/53/EC), the EU Commission banned the use of hexavalent chromium compounds in the automotive industry. As a matter of fact, the identification of new environmentally friendly surface preparation techniques is a subject of critical importance in past and present research activities.

An ecological alternative to chemical treatments is offered by the use of modern lasers. There is a growing amount of published works which testify the potential of laser irradiation to improve the bonding strength of adhesive joints. Laser surface treatment has been already assessed on a multitude of substrates for adhesive bonding, e.g. aluminum alloys [6,7], steel [8], copper and brass [9], titanium alloys [10,11], ceramics [12], polymer-matrix composites [13]. From this

* Corresponding author. Tel.: +966 0 2 808 2137/4923.
[1] Present address: University of Calabria, Italy.
E-mail address: marco.alfano@kaust.edu.sa (M. Alfano).

0143-7496/$ - see front matter © 2012 Elsevier Ltd. All rights reserved.
http://dx.doi.org/10.1016/j.ijadhadh.2012.03.002

standpoint, excimer lasers, e.g. KrF [12,13], XeCl [8], and solid state lasers, e.g. Nd:YAG [6,7], have been mostly employed. In these works, a remarkable increase in joint strength was observed with respect to samples with degreased substrates. The enhancement was associated to the (1) improved cleaning action of substrate surface, (2) improved wetting and (3) formation of a thermal oxide layer whose morphology allows to extend the surface available for bonding. It is worth noting that because of the fairly complexity of the laser treatment, the selection of the process parameters in previous works was mostly made in empirical fashion.

A recent contribution on the subject has been provided in [5,14]. In particular, a preliminary investigation on the effect of ytterbium (Yb) fiber laser irradiation on the strength of Al/Mg single lap joints was carried out. Increased bonding strength and maximum elongation at failure were reported with respect to samples with grit-blasted substrates. The result was addressed to the effective removal of any weak surface boundary layer which could fail prematurely under load. However, a detailed analysis regarding the effect of laser process parameters on substrate morphology and wettability was not made. In addition, similar to almost all the works mentioned above, the strength of the joints was qualified by means of the average shear stress, i.e. the ratio between the failure load and the nominal bonding area; but it should be recognized that the simplistic calculation of the average shear stress provides little or no information on other important joint properties, for instance on the bond toughness. This last is a key parameter for most structural models of joints and interfaces [15–17], therefore it is of great interest to determine its modification.

Motivated by the previous limitations, the present work aims to further assess the effect of Yb-fiber laser irradiation on the strength of Al/epoxy joints. In order to select a proper combination of the main technological laser process parameters (i.e. laser power, line spacing, scan speed), the morphological modifications and the wettability (i.e. contact angle) of treated surfaces were investigated using a Scanning Electron Microscope (SEM) and the sessile drop technique (ASTM Standard 724D). Adhesive bonded T-peel joints with laser treated substrates were then prepared and tested and, for comparison, identical samples were produced using standard grit-blasting. The T-peel joint was selected because of the ease of use and the physical resemblance to actual in-service debonding problems [18,19]. The variation of bond toughness associated to the different surface treatments was assessed. To this aim finite element simulations were carried out using the Park-Paulino-Roesler (PPR) potential based cohesive zone model of fracture [20].

2. Laser irradiation of AA6082-T6

2.1. Process description

Aluminum (AA6082T6) substrates were irradiated using a ytterbium fiber laser operated in pulsed mode (IPG, YLP1-100-100). A projective optical system directed and defocused the laser radiation on the sample surface. The morphological modification of the substrate depends on adjustable laser process parameters; the following technological parameters were investigated in this work: laser power, line speed and spacing. The laser process involved multiple scans over the sample surface at variable scan speed (V) and line spacing (LS), considering two power levels (P). The parameters considered for the experiments are summarized in Table 1. A schematic depiction of the laser scanning process and the investigated combinations of V, P and LS are given in Fig. 1. The process was carried out at ambient temperature and in an atmospheric environment.

Table 1
Laser process parameters employed for substrate surface irradiation.

Process parameter	Value
Laser wavelength, nm	1064
Pulse repetition rate, kHz	100
Pulse width, ns	150
Pulse energy, mJ	1
Average power (P), W	40/100
Scan speed (V), mm/s	500/750/1000
Programmed line spacing (LS), mm	0.05/0.10/0.15

2.2. SEM observations of treated surfaces

A Scanning Electron Microscope (FEI NOVA NanoSEM 630 FESEM) was used for a qualitative analysis of the laser-treated surfaces. In particular, selected SEM observations are reported in Fig. 2. As produced and grit blasted surfaces are also reported for comparison in Fig. 2(a) and (b). The surface of as produced Al substrates is almost flat, however after grit blasting random ridges and grooves were produced. The surface roughness is clearly increased, although there are little indications of crevices and pits prone to the enhancement of mechanical interlocking.

Using laser irradiation a fraction of the laser beam energy is absorbed by the material, thus promoting material melting, surface morphological modifications and the formation of a thermal oxide layer. The comparison among the SEM pictures reported in Fig. 2 demonstrates the effect of the laser process parameters. For instance, Fig. 2(c) and (f) illustrates the effect of the average power (P) on the resulting surface morphology. Specifically, laser powers of 40 W and 100 W were employed, while the other process parameters where set equal to $LS = 150\ \mu m$ and $V = 1000$ mm/s. The SEM observations demonstrate that the level of surface modification is strongly affected by the laser power. Indeed, at 100 W extensive morphological modifications are generated. On the other hand, at 40 W substrate surface is relatively unaffected by the process, and only a partial melting can be observed. For this reason, the subsequent analyses are referred to the higher power level.

If we now compare Fig. 2(d) and (e) we can appreciate the effect of increasing the laser spacing, from 50 μm to 150 μm, on the resulting surface morphology. For the smaller laser spacing it is not possible to distinguish the different laser scans made during the process. On the other hand, if the spacing is increased the formation of surface patterns becomes remarkable; in addition, the presence of a multitude of sharp asperities and oxide particles can be observed. These last formed during the process for the rapid condensation of the expanding gas or plasma during cooling [5]. Finally, comparing Fig. 2(e) and (f) one can appreciate the effect of laser speed when the spacing is held constant at 150 μm. When the speed increases from 500 to 1000 mm/s, the depth of the pattern decreases because the time available for the laser beam to heat substrate surface decreases. In order to understand how the variation of surface morphology affects wettability the analysis of contact angle is discussed next.

3. Wettability of treated surfaces

3.1. Theoretical background

When a liquid drop is brought in contact with a solid surface and rests in equilibrium on it, the molecular forces acting at the interfaces must balance according to the Young's equation which

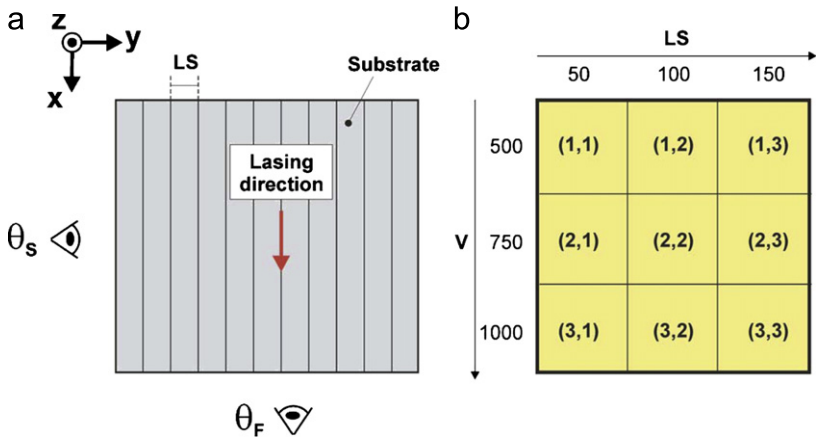

Fig. 1. (a) Schematic representation of the laser scanning direction over the sample surface and (b) associated combinations of the investigated process parameters. θ_S and θ_F denote the contact angles determined in the side and front directions.

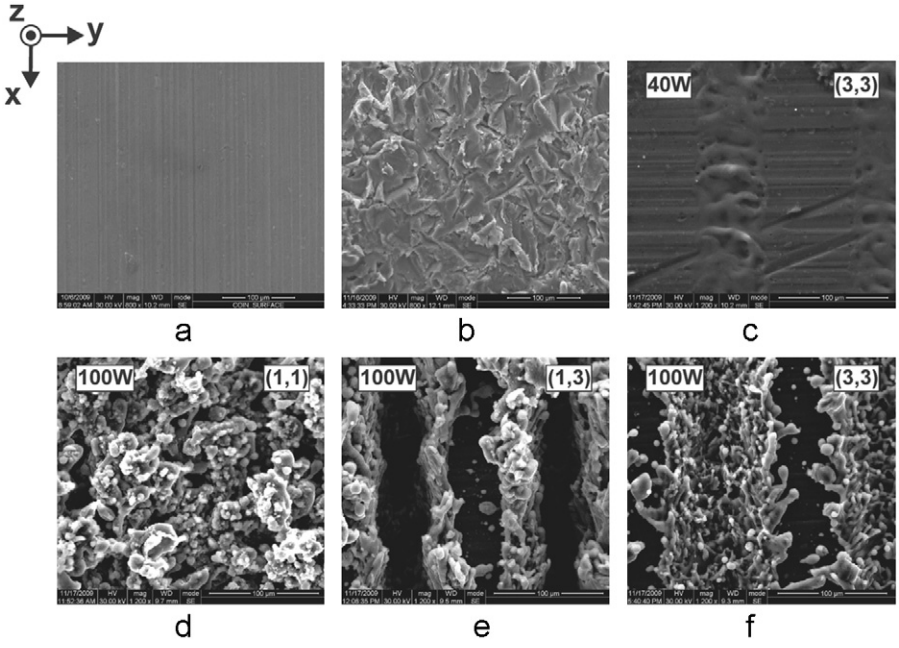

Fig. 2. SEM observations of (a) as-produced surface; (b) grit blasted surface; laser treated surface with (c) $P=40$ W, LS = 150 μm, $V=1000$ mm/s, (d) $P=100$ W, LS = 50 μm, $V=500$ mm/s, (e) $P=100$ W, LS = 150 μm, $V=500$ mm/s, (f) $P=100$ W, LS = 150 μm, $V=1000$ mm/s. The laser beam was directed in the x-direction, i.e. from top to bottom.

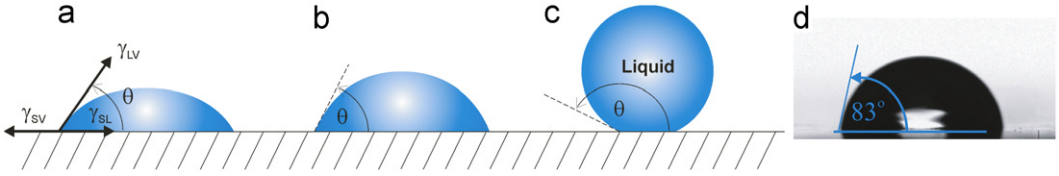

Fig. 3. (a) Equilibrium shape of a small liquid drop (L) deposited on a solid surface (S) in the presence of its vapor (V). The contact angle results from the balance of surface tensions at the three phase point of contact. (b) Contact angle for a liquid drop resting on a hydrophilic (θ less than 90°) and (c) hydrophobic (θ greater than 90°) surfaces. (d) Contact angle of a glycerol drop on as produced AA6082T6 surface.

is given as follows [1,2] (cfr. Fig. 3 (a)):

$$\gamma_{SV} = \gamma_{LV} \cos\theta + \gamma_{SL}, \quad (1)$$

where γ_{SV} and γ_{LV} are the surface energy of the solid–vapor and liquid–vapor interface, γ_{SL} is the surface energy of the solid-liquid (SL) interface and θ is the contact angle which the liquid subtends with the solid. Therefore, the final shape of the liquid drop (i.e. wetting) will depend upon the relative magnitudes of the forces existing at the three phase point of contact shown in Fig. 3(a). If the liquid wets the surface properly, it will spread to form a very low contact angle (θ). This means that wettability of a surface could be assessed from the contact angle qualitatively. As shown in Fig. 3(b) and (c), wetting occurs when θ is less than 90°, instead if θ is greater than 90° then the liquid does not wet the surface. Clearly, to achieve wetting γ_{SV} should be large, while γ_{SL} and γ_{LV} should be small. It follows that for a given surface

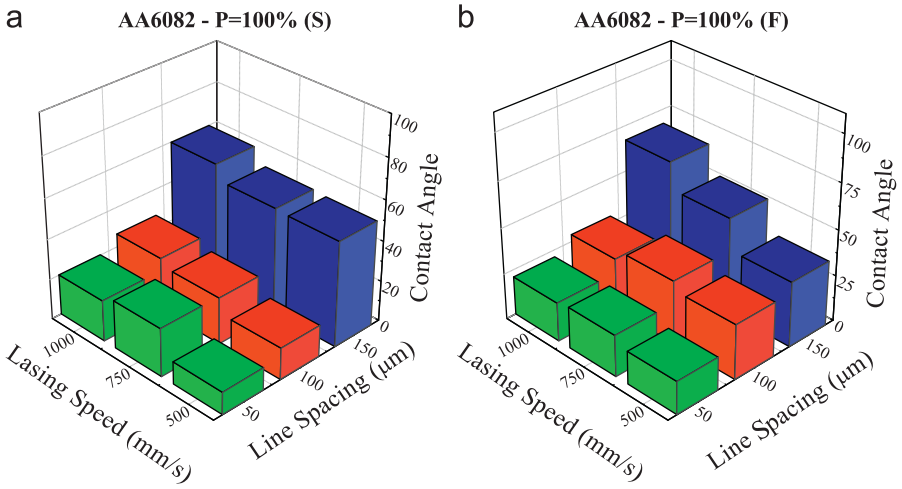

Fig. 4. Variation in contact angle as a function of the laser process parameters for a glycerol liquid drop resting on AA6082T6 laser treated surfaces taken in the (a) side and (b) front directions (cf. Fig. 2).

tension, liquids will spread easily over solid surface with higher surface tension.

It is worth noting that surface roughness may affect wettability of a solid surface. Many attempts to model the effect of surface roughness on the contact angle with liquids have been carried out. In the treatment proposed by Wenzel [1,2] a parameter r was introduced in order to characterize the contact angle of a rough surface. It is defined as the ratio of the actual (A) to the projection area (A_0) of the solid. In particular the contact angle for a given liquid on a rough surface, θ_f is expressed as follows:

$$\cos\theta_f = \frac{A}{A_0}\cos\theta_s = r\cos\theta_s, \quad (2)$$

where θ_s is the contact angle observed on a smooth surface. Therefore, according to Wenzel's model, increasing the roughness will always amplify the current wettability regime, i.e. an hydrophilic surface will become more hydrophilic and vice versa.

Therefore, if θ_s is less than 90°, then roughening the surface (r increases) will result in θ_f being even smaller, thereby providing an improved wetting. Conversely, for a smooth hydrophobic surface, i.e. θ_s greater than 90°, the roughening will further increase the contact angle and then decrease the wettability.

3.2. Experimental determination of contact angle

The analysis of contact angle can be very informative in order to assess the cleanliness of solid surface and to qualify the effectiveness of a surface pre-treatment [1]. The contact angle, θ, was measured using an optical contact angle meter (CAM 200, KSV Instruments Ltd, Finland). Glycerol drops were employed as testing liquid on as produced and laser treated samples. Note that for a given liquid, the value of θ at any time instant is affected by the spreading of the liquid drop, which in turn depends on the surface topography of the substrate. The contact angle may decrease with time owing to the penetration of the liquid in the asperities of the substrate. In order to spread out capillarity effects, measurements were carried out by means of drop shape analyses considering a 25-frame movie ($\approx$20 s duration) collected after drop deposition on sample surface. As a consequence, the values of θ quoted herein are referred to the equilibrium advancing contact angle, i.e. the values recorded toward the end of the above mentioned time interval.

The contact angle which the liquid drop formed with the as produced surface is shown in Fig. 3(d). A value equal to 83° was recorded before any surface preparation. The values of θ determined on laser treated surfaces for different combinations of laser process parameters are reported in Fig. 4. In particular, owing to the peculiar topography which can be delivered by the process, the liquid drop may be elongated in the direction of the laser scan (anisotropic wetting). For this reason, the contact angle was determined in the front (θ_F) and side (θ_S) directions (cf. Fig. 1). We note that the values of θ_F and θ_S recorded for combinations of the laser process parameters included in the ranges LS = 50−100 μm and V = 500–1000 mm/s are quite similar and are lower with respect to that measured on the as produced surface.[1]

The variation in θ conforms with the Wenzel regime, indeed, following to sample roughening by means of the laser process an increase in wetting (reduction of θ) was observed. However, for the surfaces obtained at the highest laser spacing (the patterned ones), no matter the laser speed, the contact angle is much closer to that measured on as produced substrates. Waugh et al. [21] observed a similar behavior on patterned nylon 6,6 substrates. They stated that a change from Wenzel regime to a mixed state wetting regime affected the measured contact angle. The mixed state is a mixture of Wenzel and Cassie–Baxter regimes. According to the latter, a liquid drop may rest upon the roughened surface peaks forming air-gaps with the underlying surface patterns, giving rise to a higher contact angle [22].

In order to pre-treat the substrates employed for the fabrication of the T-peel joints the combination of process parameters denoted by (2,1) in Fig. 2 was chosen. It belongs to the range of process conditions outlined above and which provided improved wetting and also prevented surface patterning. Fig. 5 illustrates the values of θ_F and θ_S, as a function of time, for this combination of process parameters; the values of contact angles obtained for as produced and grit blasted surface are reported for comparison. These results clearly show that the values of θ in the front and side direction are almost identical, and that there is a substantial improvement of wetting for the laser treated surface with respect to as produced and grit blasted samples.

[1] Note that wettability was also investigated for the surfaces treated at the lower power level (40 W); however, the contact angles showed a slight sensitivity to laser spacing and speed, indeed surface modifications made with different combination of laser parameters delivered essentially the same results in the front (F) and side (S) directions. On the average $\theta = 75°$ was recorded.

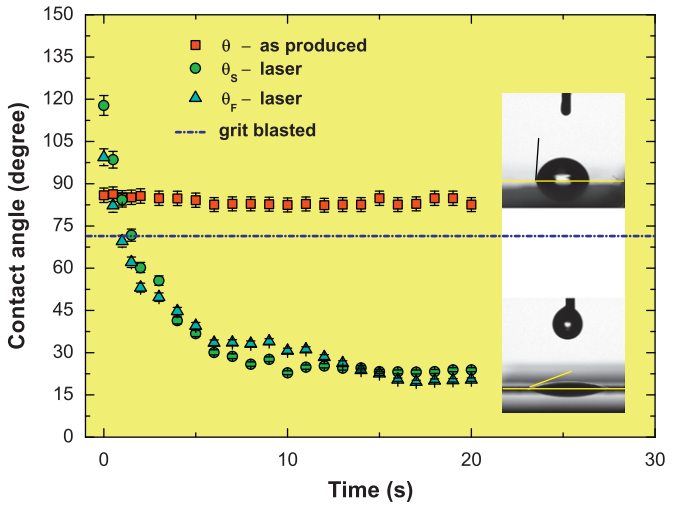

Fig. 5. Comparison among the contact angles for as produced, grit blasted and laser treated substrates. The combination of laser process parameters to which the results are referring to is as follows: $P=100$ W, LS $=50$ μm, $V=750$ mm/s. The insets in the graph show the liquid glycerol drop before and after the laser process.

4. Mechanical testing of T-peel joints

4.1. Joint preparation and testing

The joint analyzed in the present work is a T-peel aluminum (AA6082T6) joint bonded with a toughened, industrial grade bi-component epoxy adhesive (Loctite Hysol 9466). According to the manufacturer data sheet, the fully cured adhesive is able to provide high peel resistance and high shear strength; the Young modulus, determined using the ISO 527-3 standard procedures, is $E_a=1.7$ GPa [23] while the Poisson ratio is assumed to be $\nu_a=0.35$ [2]. It is worth noting that the Hysol 9466 has been already employed in previous related works and additional technical information are given in the published literature. For instance in [24], tensile static tests were performed on bulk samples and limited plasticity was observed thus denoting an essentially brittle behavior. The mechanical stress–strain curve of the aluminum alloy was determined by means of tensile tests [25]. The geometrical dimensions and boundary conditions of the T-peel joint are schematically depicted in Fig. 6. The thickness of the adhesive layer was set to 0.25 mm by using metallic spacers. The specimens were cured according to the manufacturers specifications, i.e. 7 days at 22 °C in normal atmospheric conditions, to avoid the occurrence of significant residual stresses.

Prior to bonding, samples substrates were surface treated in order to enhance the adhesion at the metal/polymer interface. As stated in the previous section, the selected combination of laser process parameters was $P=100$ W, LS $=50$ μm, $V=750$ mm/s. Laser irradiation was projected on a rectangular bonding area equal to 45×25 mm^2. The subsequent mechanical tests were performed under quasi-static loading conditions using a universal testing machine (Instron 8500 plus). The load was imposed under displacement control with a cross-head speed rate of 0.02 mm/s. For the sake of comparison samples with grit blasted (alumina grit 80) substrates were prepared and tested. To ensure statistical reliability, a series of five specimens was bonded for each surface preparation process.

The experimentally determined peel force versus displacement curves of grit blasted and laser treated samples are reported in Fig. 7. The results show an increase in maximum load and elongation at failure for laser treated samples. Owing to the improved adhesion at the metal/polymer interface, extensive substrates plastic deformations occurred before final failure. The higher scatter observed in the P-δ curves for grit blasted samples can be addressed to the poor reproducibility of this surface treatment.

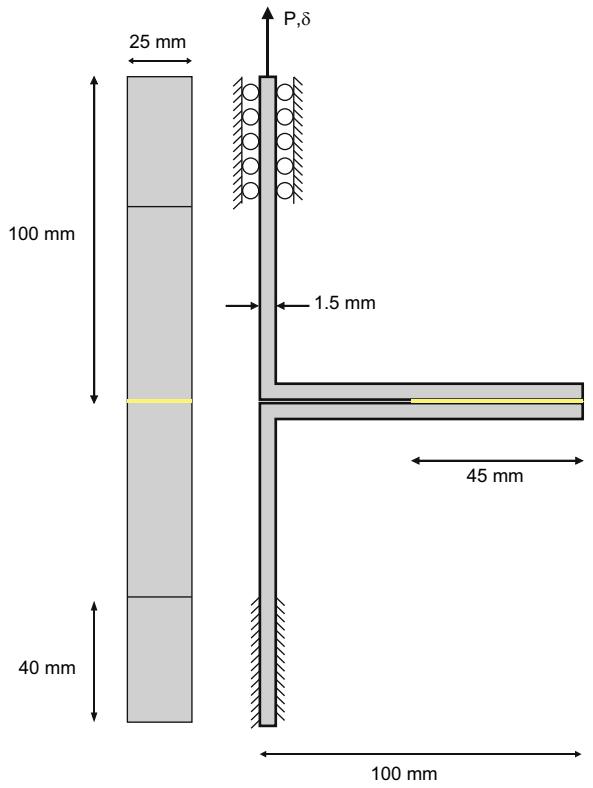

Fig. 6. Geometry and boundary conditions of the T-peel Al/epoxy sample employed in order to assess the effect of laser irradiation on the bonding strength. The radius of curvature in the bent portion of the substrates is 10 mm.

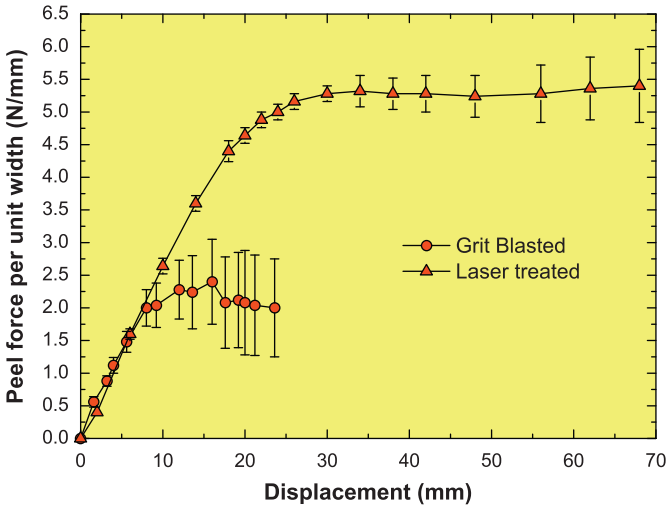

Fig. 7. Load displacement curves for the T-peel joints with grit blasted and laser treated substrates. The error bars are referred to the scatter observed over five consecutive measurements.

4.2. Analysis of failure surfaces

In order to clarify the difference observed in joints response, fracture surfaces were analyzed in detail. A post failure visual inspection revealed a fundamental difference in the mechanism of failure: fracture was adhesive (i.e. interfacial) for the joints with grit blasted substrates and cohesive for those with laser irradiated substrates. The visual inspection also revealed that in the course of interfacial fracture the failure path occasionally shifted from the upper to the lower interface and *vice versa*. This is schematically illustrated in Fig. 8(a). On the other hand, cohesive failures

occurred with the main crack running closer to one interface and then leaving a layer of adhesive on both fracture surfaces; however one surface retained more adhesive than the other. The situation is depicted in Fig. 8(b).

The fracture surfaces were also analyzed using a Scanning Electron Microscope operated under low vacuum conditions. The specific points probed during the SEM analyses are schematically illustrated in Fig. 8. In particular, Fig. 9(a–c) shows the fracture surfaces of the joints with grit blasted substrates. The failure surface observed from adhesive side, Fig. 9(a), is basically a replica of the morphological features of the grit blasted substrate. On the other hand, the SEM image taken from substrate side, Fig. 9(b) and (c), shows a bare surface. These results confirm that the mechanical pre-treatment carried out by means of standard grit blasting was not able to promote a strong interaction at the substrate/adhesive interface.

Similar analyses were carried out for the laser treated substrates and are reported in Fig. 9(d–f). Comparing Fig. 9(d) and (e), it is possible to confirm that fracture was cohesive in the adhesive layer, indeed significant portion of adhesive interlocked in the Al substrate can be appreciated. In particular, Fig. 9(d) shows the failure surface from the adhesive side. The arrows indicate Al globular oxide particles formed during the laser process which detached from the mating substrate. These particles are also observed in Fig. 2. The voids observed on the fracture surfaces, i.e. Fig. 9(e) and (f), may be addressed to the presence of air trapped during dispensing of the adhesive. On the other end Fig. 9(e) shows the failure surface from the substrate side. The arrows point on typical substrate micron sized features which nicely interlock with the adhesive. The detail enclosed by the square area in Fig. 9(e), which is shown at higher magnification in Fig. 9(f), demonstrate the highly strained area where cohesive fracture of the adhesive can be observed (the lower arrows); the upper arrow points to a typical region showing imperfect wetting at adhesive/substrate interface. This issue can be explained in terms of the specific interaction between the cold curing adhesive employed for bonding and the surface asperities created during the surface treatment. Indeed, the surface roughness can affect the spreading of the adhesive, because it cannot fully penetrate the adherent and/or it gels before a complete penetration. From this standpoint capillarity forces and adhesive viscosity may play an important role. Finally, it is instructive to note that mechanical tests carried out on single lap joints with nominally identical substrates and laser surface treatment showed near interfacial fracture without the occurrence of significant mechanical interlocking [5]. However, this result is not surprising, indeed it is well known that the locus of failure and the crack propagation behavior also depend on the mode mixity of external loads; failure tends to be more interfacial as the mode II component of the load (i.e. shear) increases [26].

5. Simulation of debonding using a potential based cohesive model

5.1. Theoretical background and modeling approach

Based on the SEM observations reported in the previous section, it is possible to infer that the improved peel load of the laser treated joints is a direct consequence of the increased surface area available for bonding and sites of mechanical keying between the adherents and the adhesive. It is now interesting to quantify the enhancement of bond toughness. Note that laser treated samples failed with extensive plastic deformation of the metal substrates owing to the improved adhesion at the adhesive/substrate interface. However, the intrinsic bond toughness of the joints is associated with the energy dissipated within the adhesive layer and it is distinct from the total energy absorbed, which includes the contribution of the plastic deformation of the adherents. Incorporating a cohesive zone model (CZM) of fracture into non-linear finite element simulations which account for plasticity in the metal substrates, the energy dissipated by plasticity can be segregated from that absorbed during fracture of the adhesive layer.

In the present paper the debonding process of the T-peel joints was simulated using a potential based cohesive model, namely the PPR (Park–Paulino–Roesler) potential based cohesive model [20,27]. In the case of mode I fracture, the intrinsic cohesive zone model for the normal cohesive stress, σ_n, is obtained as the first derivative of the potential, $\Psi(\Delta_n)$, with respect to the opening displacement Δ_n and is given as follows:

$$\sigma_n = \frac{\partial \Psi}{\partial \Delta_n} = \frac{\phi_n}{\delta_n}\left(\frac{\alpha}{m}\right)^m \left(1-\frac{\Delta_n}{\delta_n}\right)^{\alpha-1} \times \left(\frac{m}{\alpha}+\frac{\Delta_n}{\delta_n}\right)^{m-1}(\alpha+m)\frac{\Delta_n}{\delta_n}, \quad (3)$$

where ϕ_n is the mode I fracture energy, m is a non-dimensional exponent and α is the shape parameter which controls the shape of the softening branch of the cohesive model; the final crack opening width δ_n is given by

$$\delta_n = \frac{\phi_n}{\sigma_{max}}\alpha\lambda_n(1-\lambda_n)^{\alpha-1}\left(\frac{\alpha}{m}+1\right)\left(\frac{\alpha}{m}\lambda_n+1\right)^{m-1}, \quad (4)$$

where σ_{max} is the cohesive strength and λ_n is the slope indicator, which controls the initial stiffness of the model [20,27]. When the normal opening displacement equals the final crack opening width, the normal cohesive interaction is set to zero. It is worth noting that in our model there are four independent cohesive parameters which need to be determined: cohesive strength (σ_{max}), fracture energy (ϕ_n), shape parameter (α) and slope indicator (λ_n).

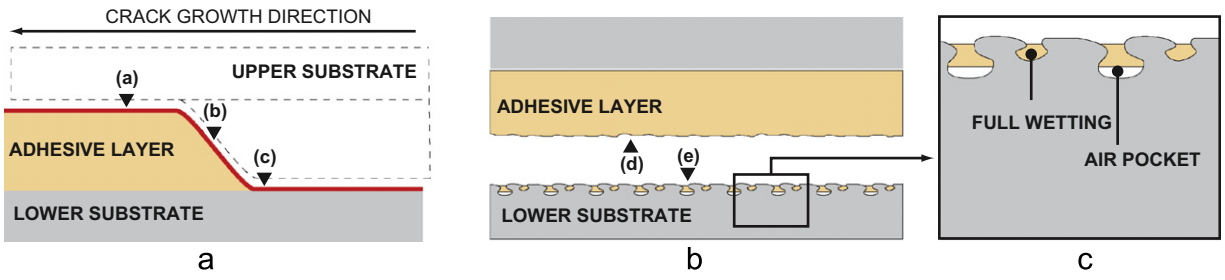

Fig. 8. Schematic depiction of fracture surfaces for samples with (a) grit blasted and (b) laser irradiated substrates showing the failure path through the joints and the locations of SEM observations. (c) Schematic of the observed mechanism of adhesive wetting illustrating areas of full wetting and the formation of air pockets on substrate surface (the drawings are not to scale).

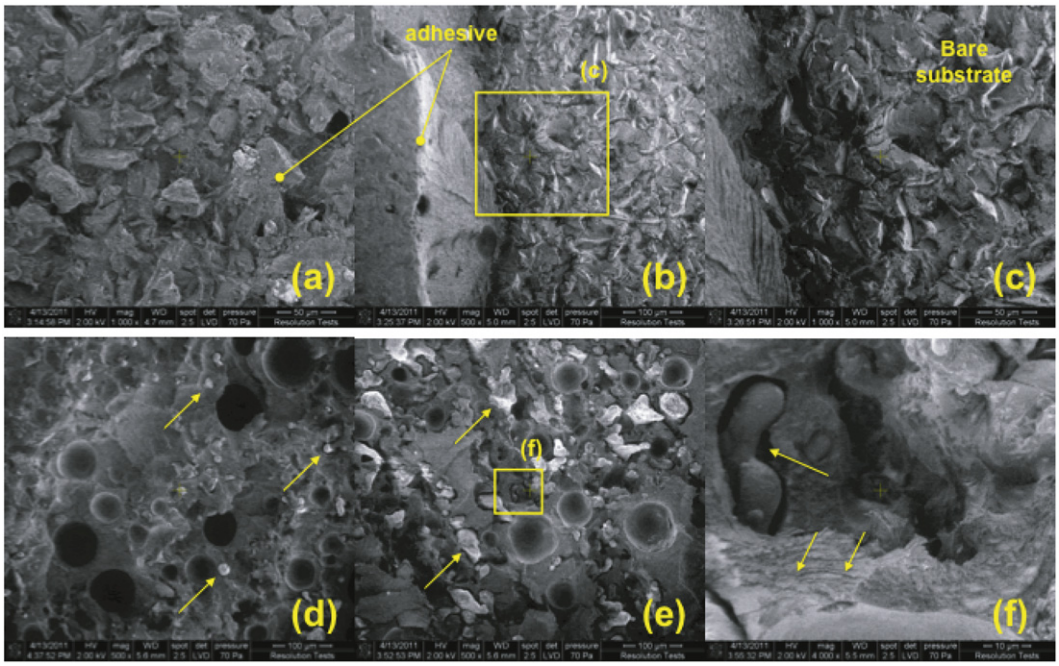

Fig. 9. SEM observations of fracture surfaces. The locations of the point probed on samples surface are schematically illustrated in Fig. 8.

A cohesive element embedding the potential based cohesive model was implemented in ABAQUS Standard. Details concerning the implementation and the finite element model are reported elsewhere [27,28] and only the key features are summarized herein. The specimen was modeled using plane-strain four-nodes continuum elements for the bulk material, and the stress–strain curve of the Al alloy was employed as input for the numerical simulations. In particular, the tensile behavior was generalized to multi-axial stress states assuming isotropic hardening and using the von Mises yield surface. Similar to the work reported in [15,16,29,30], the entire adhesive layer was replaced by a single row of cohesive elements. It is assumed that the role of the adhesive layer is to provide a traction-separation relation across the interface between the two adherends [29]. Notice that the bond toughness of the joint usually includes the energy required to overcome the intrinsic bonding forces, the energy associated to microcracking of the adhesive layer, and the plastic (or visco-elastic) energy dissipation eventually occurring in the course of fracture [16]. Replacing the adhesive layer by a single row of cohesive elements, the above mentioned energy contributing terms are directly embodied in the traction-separation relation. This modeling approach has been employed successfully for thin adhesive layers and moderately though adhesives, i.e. when the plastic dissipation is small compared to the intrinsic work of fracture [29,15,16]. The previous conditions actually conform with the epoxy adhesive employed in our experiments.

It should be also noted that the position of the crack path in the adhesive layer directly affects the significance of ϕ_n and σ_{max}. When using grit blasted substrates fracture occurs at the Al/epoxy interface, therefore ϕ_n and σ_{max} are regarded as characteristic properties of the interface. However, samples with laser irradiated substrates failed within the adhesive layer as a consequence of the improved adhesion at the interface. It follows that the previous cohesive properties should be regarded as characteristic of the adhesive layer.

5.2. Results and discussion

The parameters of the PPR were identified comparing the global measured peel-force *versus* displacement curves with the numerical counterpart obtained through the finite element simulations. This is an example of global approach in which the cohesive properties are identified by iteratively adjusting finite element predictions (e.g. load-displacement curves, deflections and/or deformed shape of the sample) to the corresponding experimental quantities [29,31]. Local approaches are based on a similar inverse procedure but make use of full field sets of surface opening displacement taken in the near crack tip region [32].

Local approaches can provide precise information on the shape of the traction separation relation, however a detailed knowledge of the cohesive model may not always be necessary for predictive modeling of plastically deforming adhesive joints. For instance the work by Yang et al [29] showed that the prediction of macroscopic load-displacement curves, or deformed shape of the sample, the cohesive strength and cohesive energy were the only information needed and that the shape of the cohesive model was of secondary importance. A sensitivity analysis to cohesive fracture parameters carried out in [27,33] provided results in agreement with the previous statements, indeed the λ_n and α had a negligible influence on the global load displacement curve. For this reason these parameters were set equal to $\alpha = 3$ and $\lambda_n = 0.06$, respectively. Therefore, iterations have been made to identify the values of ϕ_n and σ_{max} providing a reasonable match between experiments and simulations. The results which provided the best fit with the experiments are reported in Fig. 10. It is apparent that there are different combinations of ϕ_n and σ_{max} which can provide a reasonable match between experiments and simulations.

This non-uniqueness of the identified values of ϕ_n and σ_{max} was investigated by the authors in a separate contribution [33]. In particular, a cost function which quantifies the difference between numerical predictions and experimental load–displacement curves was defined. A sensitivity analysis of the cost function demonstrated that there is a low sensitivity of the simulated global load–displacement curve to cohesive strength while a reasonable identification of cohesive energy could be carried out based on global data. Therefore the analysis of the results reported in Fig. 10 allows us to infer that, on the average, the bond toughness for the joints with laser irradiated substrates was up to four times greater than that of the joints with grit blasted substrates.

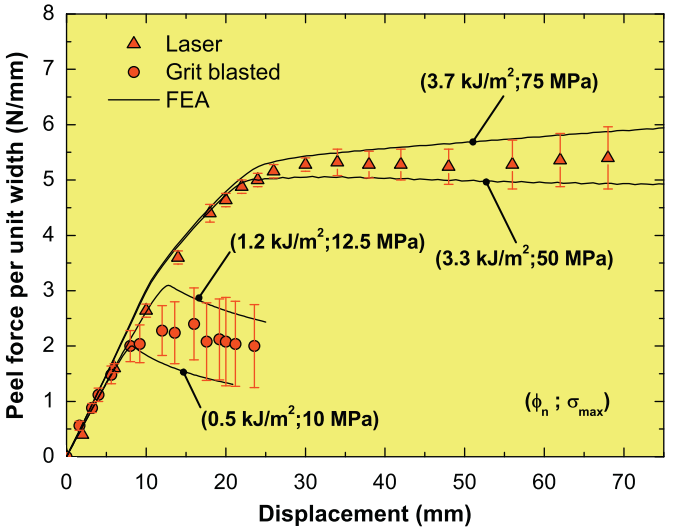

Fig. 10. Comparison between numerical and experimental force *versus* displacement curves for T-peel sample with grit blasted and laser irradiated substrates.

However, it is recognized that the transferability of the present laboratory results to different joints design can be troublesome because of the existence of constraint effects. Specifically, Kafkalidis et al. [31] demonstrated that the cohesive strength of plastically deforming adhesive joints is affected by the constraint level in the joint. In other words, they showed that σ_{max} decreases for increasing thickness of the adhesive layer or decreasing thickness of the adherents. As a result, adhesive joints made-up with nominally identical materials and fabrications procedures, may show different values of σ_{max} according to the specific constraint level. On the other hand, the variation in σ_{max} and δ_n was such that the cohesive energy remained approximately constant. For this reason we expect the identified range of ϕ_n to be fairly representative of the mode I bond toughness of the joint and that, in principle, could be employed for predictive modeling of similar joints made up with nominally identical materials and similar bond-line thickness.

In order to cross-check the so obtained values of the fracture energy the test protocol described in [34] was employed. The test protocol provides guidance on conducting peel tests and to convert peel strength to adhesive fracture toughness. It makes use of an elastic-plastic bending solution [35] to determine the amount of plastic energy dissipated in the peeling arms. As a result, the adhesive fracture energy can be segregated from the total external energy required to generate peel fracture. Notice that precise details on the equations involved are reported in [34,35] and are omitted herein for brevity. The obtained values of adhesive fracture energy for samples with grit blasted and laser treated substrates were equal to $\approx 2.2\ \mathrm{kJ/m^2}$ and $\approx 4.3\ \mathrm{J/m^2}$, respectively. Therefore, there is a reasonable agreement between the upper bounds values of the energy reported herein and those calculated with the protocol. The main reason for the deviation between the results obtained using the protocol and the CZM can be readily understood if one recognized that the sample geometry employed in the present work does not exactly conform that considered for the theoretical analysis reported in [35]. Indeed, there is a relatively large un-bonded portion (Fig. 6) which undergoes elastic and/or plastic deformation in the course of fracture. These deformations give raise to an additional contribution to the overall stored/dissipated energy which should be removed from the fracture energy. The finite element modeling approach employed herein captures this feature thereby providing lower bound estimates.

6. Closure

The present work addressed the effect of Yb-fiber laser irradiation on aluminum substrates for adhesive bonding. The evolution of substrate surface morphology and wettability, for various sets of laser power, line spacing and scan speed, was investigated by means of SEM analysis and contact angle measurements. The results showed that the laser process ensures material removal thereby cleaning out any weak layer. Using a laser power of 100 W, there was a range of process parameters which provided enhanced wettabilty of the solid surface. However, it was noted that increasing the laser spacing has a detrimental effect on the obtained contact angle; this issue was explained in terms of a transition from Wenzel's to a mixed state wetting regime, where the liquid drop sits on substrate asperities forming air pockets.

Adhesive bonded Al/epoxy T-peel joints with laser treated substrates were prepared and tested and for comparison, identical samples were produced using grit-blasted substrates. An increased peel load was observed for laser treated samples, and a post-failure SEM analysis revealed that the morphological modifications promoted enhanced mechanical interlocking. In order to typify the increase in bond toughness of the joints, finite element simulations were carried out using a potential based cohesive zone model of fracture. The numerical results allowed us to conclude that the bond toughness of the joints with laser treated substrates can be up to four times greater than that of grit blasted samples.

We finally emphasize that the selected combination of laser parameters does not lead to any significant surface patterning. However, recent experimentations in conjunction with finite element analyses have suggested that the strength and the toughness of an interface between two materials can be enhanced by manipulating surface roughness [36–40]. In particular, it has been observed that micro-patterned surfaces can improve mechanical interlocking thereby leading to material damage and energy absorption and then to the inhibition of crack propagation (i.e. interfacial toughening). This topic will be the subject of the follow-up work.

References

[1] Adams RD, Comyn J, Wake WC. Structural adhesives joints in engineering. Chapman and Hall; 1997.
[2] Kinloch AJ. Adhesion and adhesives, science and technology. Chapman and Hall; 1987.
[3] Da Silva LFM, Ochsner A, Adams RD. Handbook of adhesion technology. Springer; 2011.
[4] Critchlow GW, Brewis DM. Review of surface pretreatments for aluminium alloys. Int J Adhes Adhes 1996;16:255–74.
[5] Alfano M, Ambrogio G, Crea F, Filice L, Furgiuele F. Influence of laser surface modification on bonding strength of Al/Mg adhesive joints. J Adh Sci Technol 2011;25(11):1261–76.
[6] Wong RCP, Hoult AP, Kim JK, Yu TX. Improvement of adhesive bonding alloys using a laser surface texturing process. J Mater Process Technol 1997;63:579–84.
[7] Rechner R, Jansen I, Beyer E. Influence on the strength and aging resistance of aluminum joints by laser pre-treatment and surface modification. Int J Adhes Adhes 2010;30(7):595–601.
[8] Jahani HR, Moffat B, Mueller RE, Fumo D, Duley W, North T, Gu B. Excimer laser surface modification of coated steel for enhancement of adhesive bonding. Appl Surf Sci 1998;127–129:767–72.
[9] Henari F, Blau W. Excimer-laser surface treatment of metals for improved adhesion. Appl Opt 1995;34:581–4.
[10] Baburaj EG, Starikov D, Evans J, Shafeev GA, Bensaoula A. Enhancement of adhesive joint strength by laser surface modification. Int J Adhes Adhes 2007;27(4):268–76.
[11] Man HC, Zhao NQ. Enhancing the adhesive bonding strength of NiTi shape memory alloys by laser gas nitriding and selective etching. Appl Surf Sci 2006;253:1595–600.
[12] Man HC, Zhang XM, Yue TM, Lau WS. Excimer laser surface modification of engineering ceramics for adhesive bonding. J Mater Process Technol 1997;66:123–9.

[13] Park JK, Mukherjee K. Excimer laser surface treatment of sheet molding compound for adhesive bonding. Mater Manuf Process 1998;13:359–68.
[14] Alfano M, Ambrogio G, Filice L, Furgiuele F, Gallus E, D'Antuoni D. On the performance of welded, riveted and adhesive bonded Al/Mg sheet metal joints. Key Eng Mat 2011;473:237–42.
[15] Alfano M, Furgiuele F, Leonardi A, Maletta C, Paulino GH. Mode I fracture of adhesive joints using tailored cohesive zone models. Int J Fract 2009;157:193–204.
[16] Alfano M, Furgiuele F, Pagnotta L, Paulino GH. Analysis of fracture in aluminum joints bonded with a bi-component epoxy adhesive. J Test and Eval 2011;39(2):JTE102753.
[17] Ladeveze P, Lubineau G. Relationships between micro and meso mechanics of laminated composites - Pont entre les micro et meso mecaniques des composites stratifies. Comptes Rendus Mecanique 2003;331(8):537–44.
[18] Grant LDR, da Silva LFM, Adams RD. Effect of the temperature on the strength of adhesively bonded single lap and T joints for the automotive industry. Int J Adhes Adhes 2009;29(5):535–42.
[19] da Silva LFM, Adams RD. The strength of adhesively bonded T-joints. Int J Adhes Adhes 2002;22(4):311–5.
[20] Park K, Paulino GH, Roesler JR. A unified potential-based cohesive model of mixed-mode fracture. J Mech Phys Solids 2009;57:891–908.
[21] Waugh DG, Lawrence J, Walton CD, Zakaria RB. On the effects of using CO_2 and F_2 lasers to modify the wettability of a polymeric biomaterial. Opt Laser Technol 2010;42:347–56.
[22] Cassie ABD, Baxter S. Wettability of porous surfaces. Trans Faraday Soc 1944;40:546–51.
[23] Loctite Hysol 9466. Technical Data Sheet, 2006.
[24] Goglio L, Peroni L, Peroni M, Rossetto M. High strain-rate compression and tension behaviour of an epoxy bi-component adhesive. Int J Adhes Adhes 2008;28:329–39.
[25] Alfano M. King Abdullah University of Science and Technology, 2010, Technical Report (available upon request).
[26] Chen B, Dillard DA, Dillard JG, Clark Jr. RL. Crack path selection in adhesively bonded joints: the roles of external loads and specimen geometry. Int J Fract 2002;114(2):167–90.
[27] Alfano M, Lubineau G, Furgiuele F, Paulino GH. Simulation of debonding in Al/epoxy T-peel joints using a potential based cohesive zone model. Procedia Eng 2011;10:1765–70.
[28] Alfano M, Furgiuele F. Simulating fracture in bonded composite joints using cohesive zone models. In: Camanho P, Tong L, editors. Composite joints and connections: principles, modelling and testing. Cambridge, UK: Woodhead Publishing Ltd; 2011. p. 341–62.
[29] Yang QD, Thouless MD, Ward SM. Numerical simulations of adhesively bonded beams failing with extensive plastic deformation. J Mech Phys Solids 1999;47:1337–53.
[30] Högberg JL. Mixed mode cohesive models. Int J Fract 2006;141:549–59.
[31] Kafkalidis MS, Thouless MD, Yang QD, Ward SM. Deformation and fracture of an adhesive layer constrained by plastically-deforming adherends. J Adhes Sci Technol 2000;14:1593–607.
[32] Fedele R, Raka B, Hild F, Roux S. Identification of adhesive properties in GLARE assemblies using digital image correlation. J Mech Phys Solids 2009;57:1003–16.
[33] Alfano M, Lubineau G, Furgiuele F, Paulino GH. On the enhancement of bond toughness for Al/epoxy T-peel joints with laser treated substrates. Int J Fract 2011;171:139–50.
[34] Moore DR, Williams JG. A protocol for determination of the adhesive fracture toughness of flexible laminates by peel testing: fixed arm and T-peel methods. ESIS protocol, 11/2010.
[35] Kinloch AJ, Lau CC, Williams JG. The peeling of flexible laminates. Int J Fract 1994;66:45–70.
[36] Cordisco F, Zavattieri PD, Hector Jr. LG, Bower AF. Toughness of a patterned interface between two elastically dissimilar solids. Engineering Fracture Mechanics, In preparation.
[37] Zavattieri PD, Hector Jr. LG, Bower AF. Cohesive zone simulations of crack growth along a rough interface between two elastic–plastic solids. Eng Fract Mech 2008;75:4309–32.
[38] Zavattieri PD, Hector Jr. LG, Bower A. Determination of the effective mode—I toughness of a sinusoidal interface between two elastic solids. Int J Fract 2007;145:167–80.
[39] Lee MJ, Kim WS, Jang CJ. Analysis and simulation of the failure characteristic of a single leg bending joint with a micro-patterned surface. J Adhes 2011;87:826–41.
[40] Da Silva LFM, Ferreira NMAJ, Richter-Trummer V, Marques EAS. Effect of grooves on the strength of adhesively bonded joints. Int J Adhes Adhes 2010;30:735–43.